DOI：10.1088/1361-6528/abc288

Strain-engineered black arsenene as a promising gas sensor for detecting SO_2 among SF_6 decompositions

Jianjun Mao[1] and Yue Chen[1,2*]

[1]*Department of Mechanical Engineering, The University of Hong Kong, Pokfulam Road, Hong Kong SAR, China*
[2] *HKU Zhejiang Institute of Research and Innovation, 1623 Dayuan Road, Lin An 311305, China*

Abstract: The adsorption and gas sensing properties of black arsenene (B-As) regarding sulfur hexafluoride (SF_6) and its six decompositions (SOF_2, SO_2F_2, SO_2, H_2S, HF, and CF_4) are investigated using density functional theory (DFT) combined with the nonequilibrium Green's function (NEGF). The sensitivity of B-As is evaluated by considering the most stable adsorption configuration, adsorption energy, work function, recovery time, local density of states (LDOS), and charge transfer between the gas molecules and B-As. It is demonstrated that B-As is more sensitive to the SO_2 molecule than to the other decompositions. Additionally, the adsorption strength can be manipulated by controlling the external electric field (*E*-field). The application of tensile biaxial strain results in more isotropic electrical conductance of B-As, and it can also effectively enhance the response toward SO_2. For example, under a 1% equibiaxial tensile strain, a 132% response can be obtained along the zigzag direction. This work suggests the promising prospects of B-As-based gas sensors for detecting SO_2 among SF_6 decompositions.

Keywords: Black arsenene, SF_6 decompositions, gas sensor, SO_2 adsorption, electric field, strain engineering

Introduction

* Corresponding author. Email: yuechen@hku.hk

Sulfur hexafluoride (SF_6) gas, one of the most commonly used insulation gases in the gas-insulated switchgear (GIS) and other high voltage facilities,[1] due to its preeminent chemical inertia and outstanding dielectric strength, inevitably decomposes under local discharge in a long-running apparatus.[2, 3] Reacting with air or water vapor, the decompositions then generate several constituents, such as SOF_2, SO_2F_2, H_2S, SO_2, HF, and CF_4.[4-6] A previous study demonstrated that these decompositions accelerate the corrosion of the device and can even paralyze it.[4] Furthermore, the type, concentration and formation regularity of SF_6 decompositions have a tight correlation with the seriousness of insulation failure.[7] In recent years, photoacoustic spectrometry,[8] gas chromatography,[9] and infrared absorption spectrometry[10] have been applied to detect the decomposition constituents of SF_6. Nonetheless, these methods can only monitor insulation status offline. Therefore, it is of great necessity and significance to further develop online detection of these representative decomposition gases of SF_6 to evaluate the running conditions of equipment, protecting against more serious insulation faults.

Two-dimensional (2D) materials take advantage of high surface-to-volume ratios and immediate gas substrate charge transfer, making them suitable as gas sensors.[11, 12] Graphene makes individual gas molecules detection possible.[13] However, the sp^2 hybridization of planar pristine graphene lead to inefficient gas adsorption performance, hindering its application as a gas sensor.[14] Optimization schemes such as the introduction of defects or dopants have been taken into consideration. Nevertheless, some of these modifications may be hard to control, thus affecting the sensing resolution.[15] Therefore, it is of practical importance to look for suitable adsorbent materials with enhanced gas adsorption capability. Lately, group V 2D materials (P, As, Sb, and Bi) have been intensively investigated due to not only their considerable bandgaps and high carrier mobilities[16, 17] but also their puckered or buckled structure, which may facilitate gas adsorption.[18, 19] Black (puckered) phosphorene (B-P) was first estimated to be a superior gas sensor toward NO_2 from DFT-NEGF[18] and was later experimentally realized.[20] Unfortunately, B-P tends to degrade via oxidation under ambient conditions, which heavily limits its applications.[21, 22] Recently, metastable blue phosphorene (β-P) featuring a buckled crystal structure was predicted to be a promising candidate for gas sensor.[23] Buckeld antimonene (β-Sb) has been successfully exfoliated on Bi_2Te_3 and Sb_2Te_3.[24] Besides, using a plasma-assisted process, Tsai et al.[25] synthesized the gray arsenene (β-As) multilayer nanoribbon on an InAs surface and it was shown that β-As has a remarkable sensing performance toward NO and NO_2.[26]

As a competing metastable 2D allotrope of As, B-As was first theoretically predicted[27] and then fabricated experimentally.[28] B-As shows intriguing properties, including in-plane anisotropies,[28, 29] tunable bandgaps,[27, 30] low lattice thermal conductivities,[31] and potential lateral hybridizations with other allotropes of 2D As.[32] B-As has a puckered configuration similar to that of B-P and also obtains remarkable stability.[28, 33] Furthermore, monolayer and few-layer B-As-based field effect transistors (FETs) have been realized, and layer-dependent transport properties with long-term stability have been reported for these materials.[33] Our recent work revealed that B-As shows promising anisotropic sensitivity and selectivity toward NO, NO_2, and NH_3.[29] In addition, other 2D materials namely Janus MoSSe [34] and modified green phosphorene (G-P) [35] were demonstrated to be sensitive and selective toward the decompositions of SF_6. To explore the possibilities of detecting SF_6 decompositions by B-As, a fundamental understanding of the interactions between B-As and SF_6 decompositions is critical.

In this work, to explore the use of B-As to detect SF_6 decompositions, we systematically investigated the adsorption properties, such as the adsorption energy, adsorption distance, charge transfer, work function, and recovery time. Moreover, we find that the adsorption strengths of the decompositions of SF_6 can be effectively manipulated by an external vertical *E*-field, while the adsorption strengths show limited sensitivity to tensile biaxial strains. The adsorptions of most of these molecules induce no obvious variations in the DOS near the Fermi level. To explore the feasibility of B-As for sensing SF_6 decompositions, we simulated a B-As-based gas sensing device and obtained the current-voltage (*I*-*V*) relation using the NEGF method. The results show that the adsorption of SO_2 induces an obvious response along the zigzag direction. We reveal that strain tunable anisotropic electrical conductance can be realized in B-As. Furthermore, the response of B-As to SO_2 can be enhanced under a small equibiaxial tensile strain. Our results suggest potential strategies for designing B-As-based sensors for detecting SO_2 among the decompositions of SF_6.

Computational details

Spin-polarized structural optimizations and electronic structure calculations were performed by using density functional theory (DFT), as implemented in VASP.[36] The generalized gradient approximation (GGA) with the Perdew–Burke–Ernzerhof (PBE) functional was employed to account the exchange correlation effects.[37] The electron-ion interactions were described by the projector augmented wave (PAW) method.[38] As-$4s^24p^3$, C-$2s^22p^2$, O-$2s^22p^4$, S-$3s^23p^4$, F-$2s^22p^5$, and H-$1s^1$ were treated as the valance electrons, while the remaining electrons were kept frozen as core states. The electron transport properties were computed using the TRANSIESTA package with the NEGF techniques.[39] More computational details are included in the Supplemental Material.

Results and discussion

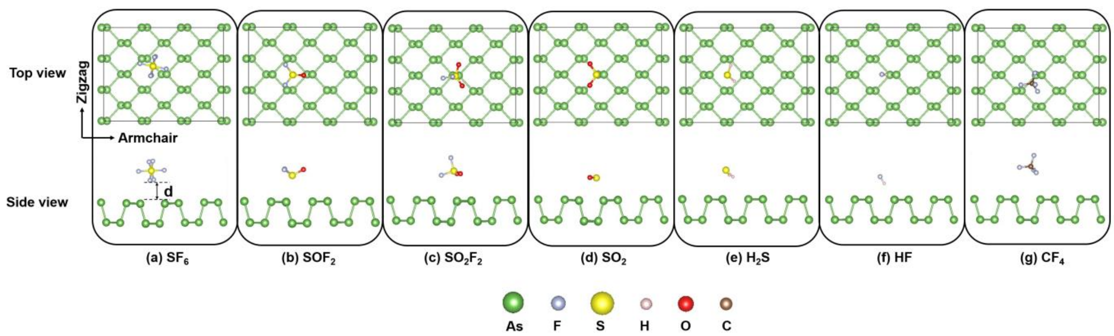

Figure 1 (color online) Optimized configurations of B-As with SF_6, SOF_2, SO_2F_2, SO_2, H_2S, HF, and CF_4 adsorption. The adsorption distance *d* between a gas molecule and B-As is defined in panel (a).

A 3×3 supercell based on a unit cell of 3.69 Å×4.75 Å is used as the substrate. To determine the favored adsorption configurations, gas molecules are initially placed at different positions on B-As with different orientations (see Figure S1 of Supplemental Material). The preferred configurations of SF_6, SOF_2, SO_2F_2, SO_2, H_2S, HF, and CF_4 molecules adsorbed on B-As are summarized in Figure 1. Detailed information, including the adsorption energy (E_{ads}), magnetism (*Mag*), Bader charge transfer (Q), adsorption distance (d) between the gas molecule and B-As, and work function (ϕ), is summarized in Table 1. SF_6 and CF_4 tend to approach the middle of the As-As bond, as shown in Figure 1 (a, g), with distances of 2.79 Å and 3.15 Å, respectively. SOF_2 and H_2S tend to have their S atoms located at the center of the honeycomb, while H_2S adopts a tilt H-end down configuration with a shorter distance (d = 2.63 Å). SO_2 tends to be adsorbed on top of the As atom, with the S-O bonds parallel to the As-As bonds. Similar configurations are observed when SO_2 is adsorbed on B-P and IV-VI group compounds (IV = Ge, Sn; VI = S, Se).[40] SO_2F_2 and HF are atop near the As atom. Similar to H_2S, the H-end down configuration is favored for HF, which has the shortest adsorption distance (1.94 Å) among all the gas molecules investigated here.

The adsorption energies for the quantitative determination of the gas adsorption strength are given in Table 1. CF_4 has the lowest adsorption strength (E_{ads} = -0.07 eV). The interaction between SO_2 and B-As is much stronger (E_{ads} = -0.48 eV), suggesting that B-As has a higher selectivity for SO_2. This adsorption strength on B-As is also comparable to that on B-P [40], GeS [40], and MoSSe [34], higher than that on G-P [35] as summarized in Table S1, indicating a potentially high sensitivity for SO_2 adsorption on B-As.

Table 1 Adsorption energy (E_{ads}), magnetism (*Mag*), Bader charge transfer (Q) with positive values indicating accepting electrons, adsorption distance (d) between the gas molecule and B-As, and work function (ϕ), as calculated from DFT.

	SF_6	SOF_2	SO_2F_2	SO_2	H_2S	HF	CF_4
E_{ads} (eV)	-0.13	-0.22	-0.21	-0.48	-0.24	-0.25	-0.07

Mag **(μ_B)**	0	0	0	0	0	0	0
Q **(e)**	0.05	0.06	0.04	0.28	0.001	0.08	0.02
d **(Å)**	2.79	2.99	2.95	2.63	2.63	1.94	3.15
ϕ (eV)	4.31	4.63	4.23	4.57	4.36	4.63	4.24

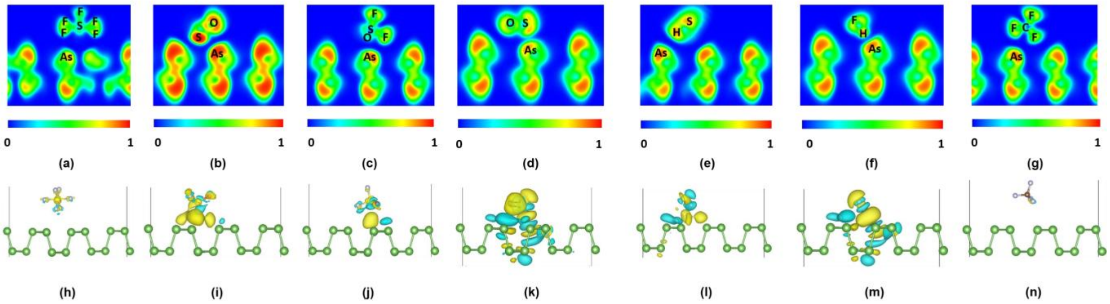

Figure 2 (color online) Electron localization function (ELF) of (a) SF_6, (b) SOF_2, (c) SO_2F_2, (d) SO_2, (e) H_2S, (f) HF, and (g) CF_4 adsorbed on B-As. Charge density difference (CDD) plots for (h) SF_6, (i) SOF_2, (j) SO_2F_2, (k) SO_2, (l) H_2S, (m) HF, and (n) CF_4 adsorbed on B-As; the yellow (blue) region represents an accumulation (depletion) of electrons. The isosurface value is taken as 0.3×10^{-3} eÅ^{-3}.

Adsorption-induced charge transfer is critical for the adsorption strength and may result in the alteration of the resistivity, making the detection of even a single molecule possible.[18, 29] Accordingly, charge transfer for the adsorption system is determined via Bader charge analysis, and the results are given in Table 1. All the molecules are found to be acceptors, and significant charge transfer is observed in SO_2, as also visualized in the charge density difference (CDD) shown in Figure 2(k). A noticeable change in the conductivity is expected due to the variation in the charge of the substrate induced by SO_2. To obtain further insight into the interaction between gas molecules and B-As, we depict the electron localization function (ELF) in Figure 2(a-g). There are no obvious electron localization overlaps between the gas molecules and B-As, suggesting a physisorption feature for these molecules, and their adsorptions may be reversible. The bond lengths of the physically adsorbed molecules are slightly longer than those of the free molecules (see Table S2). From the conventional transition state theory, the recovery time at 300 K of the molecules on B-As is given in Table S3. The adsorbed gas molecule may also be distinguished by the variation in the work function (ϕ), which is defined as $\phi = V_{vac} - E_f$ (V_{vac}: electrostatic potential of vacuum level; E_f: Fermi level). Pristine B-As has ϕ = 4.24 eV;

upon the adsorption of SOF_2, SO_2 or HF molecules, the work function is noticeably enhanced.

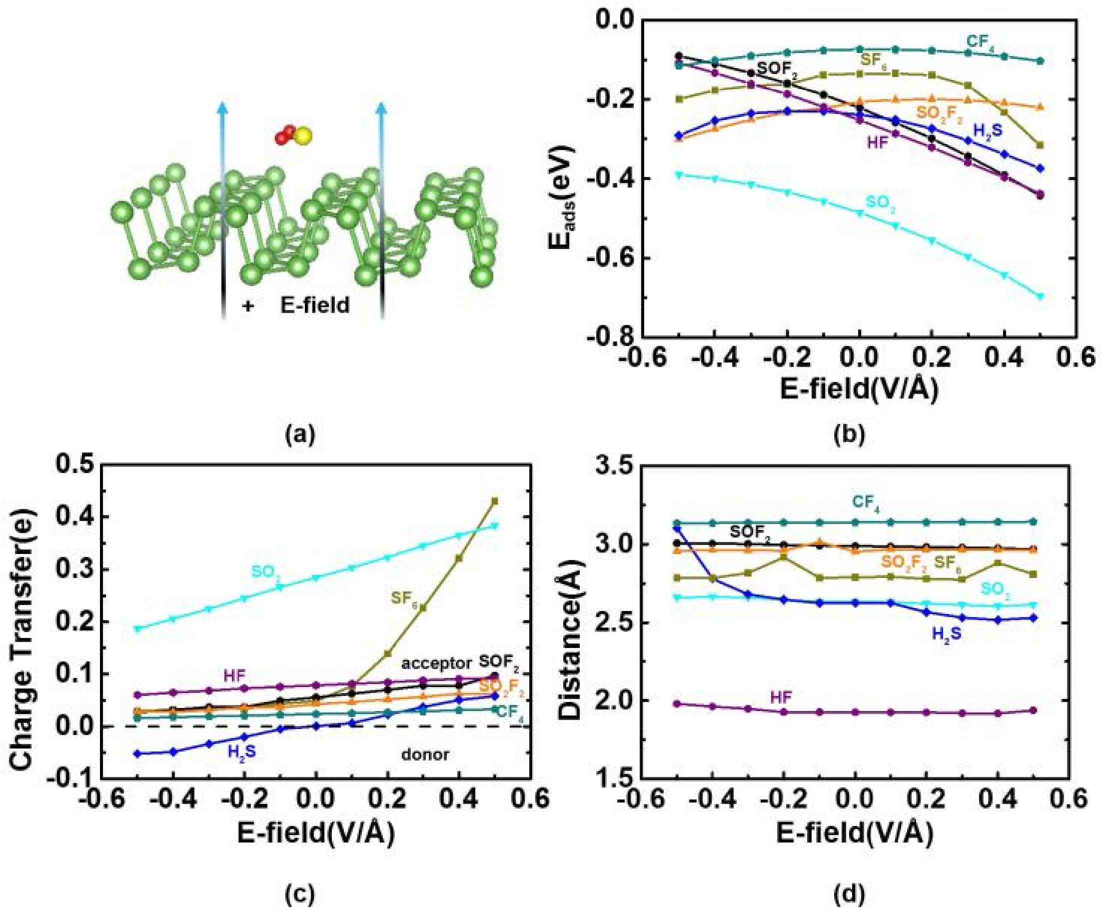

Figure 3 (color online) (a) Schematic of SO_2 adsorbed on B-As under an external positive *E*-field. Adsorption energy (b), charge transfer (c), and adsorption distance (d) as functions of the external *E*-field for SF_6, SOF_2, SO_2F_2, SO_2, H_2S, HF, and CF_4.

The gas adsorption energies can be tuned by an external *E*-field or lattice strain. The effect of the *E*-field is evidenced in a recent investigation of the adsorption of CO_2 on *h*-BN,[41] and the strain effect has been evaluated in the adsorption of NH_3 on Ti_2CO_2.[42] Our previous work revealed that *E*-fields and biaxial strain can modulate the adsorption strengths of NO and NO_2 on B-As.[29] Herein, we study the adsorption behaviors of the decompositions of SF_6 on B-As under an external *E*-field and in-plane equibiaxial tensile strain, as shown in Figures 3 and 4. The adsorption strengths of SO_2, SOF_2, and HF can be significantly enhanced under a positive *E*-field, and their affinities can be effectively tuned by changing the direction and intensity of the *E*-field. In contrast, nonmonotonic dependences are found for CF_4, SF_6, SO_2F_2, and H_2S, of which the adsorption strengths decrease first and then increase as the *E*-field changes from -0.5 VÅ^{-1} to 0.5 VÅ^{-1}. Notably, there is a sudden increase in the adsorption strength of SF_6 when the intensity of the *E*-field is larger than 0.2 VÅ^{-1}, which may be related to the distinct change in the charge transfer, as shown in Figure 3(c). Interestingly, H_2S can switch from a donor to an acceptor as the *E*-field changes from negative to positive. A similar phenomenon was reported regarding when NH_3 is adsorbed on B-As.[29] The adsorption distances of these gas molecules are shown in Figure 3(d); a weak dependence on the *E*-field is found for most molecules except H_2S, which approaches B-As as the *E*-field changes from -0.5 VÅ^{-1} to 0.5 VÅ^{-1}.

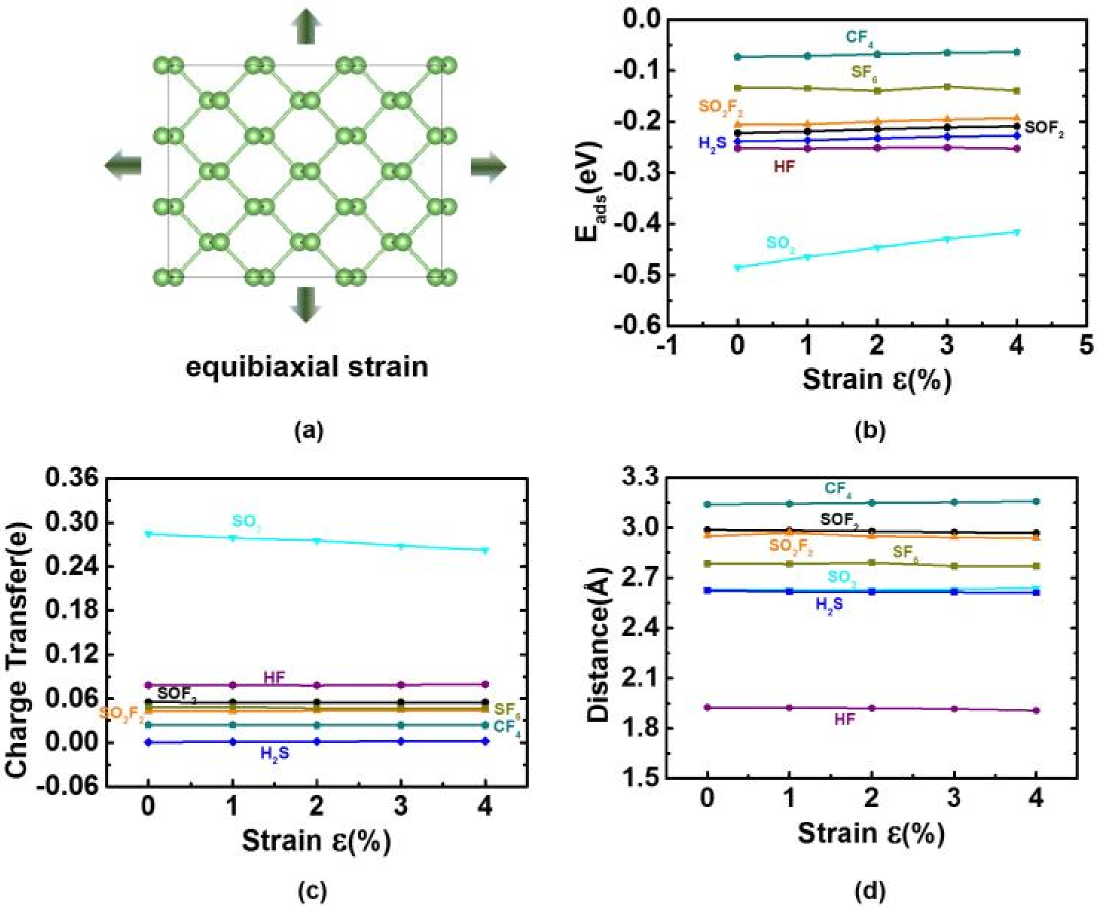

Figure 4 (color online) (a) Schematic plot of B-As under an equibiaxial tensile strain. (b) Adsorption energies, (c) charge transfers, and (d) adsorption distances of gas molecules as functions of the applied equibiaxial strain. Strained B-As has a lattice constant of $a = (1 + \varepsilon\%) \times a_o$ (a_o represents the lattice constant of pristine B-As along the *x*- or *y*-direction.).

Moreover, we have investigated the adsorption property of these gas molecules on B-As under equibiaxial tensile strains. As depicted in Figure 4(b) and (c), the adsorption strength and charge transfer of SO_2 decrease slightly under strain. In contrast, the adsorption of other molecules on B-As is less sensitive to the tensile strains; insignificant changes are found in the adsorption energy, charge transfer, and adsorption distance, as shown in Figure 4(b), (c) and (d), respectively.

As gas adsorption may modify the electronic properties of 2D materials, we calculate the total density of states (TDOS) as well as the local density of states (LDOS) projected on the gas molecules (see Figure S2). The presence of SOF_2, SO_2F_2, H_2S, HF, or CF_4 does not lead to noticeable changes in the electronic states in the vicinity of the Fermi level, whereas SO_2 and SF_6 significantly alter the electronic states near the bottom of the conduction bands. In addition, strong hybridization is observed between SO_2 and B-As, as shown in Figure S2(e).

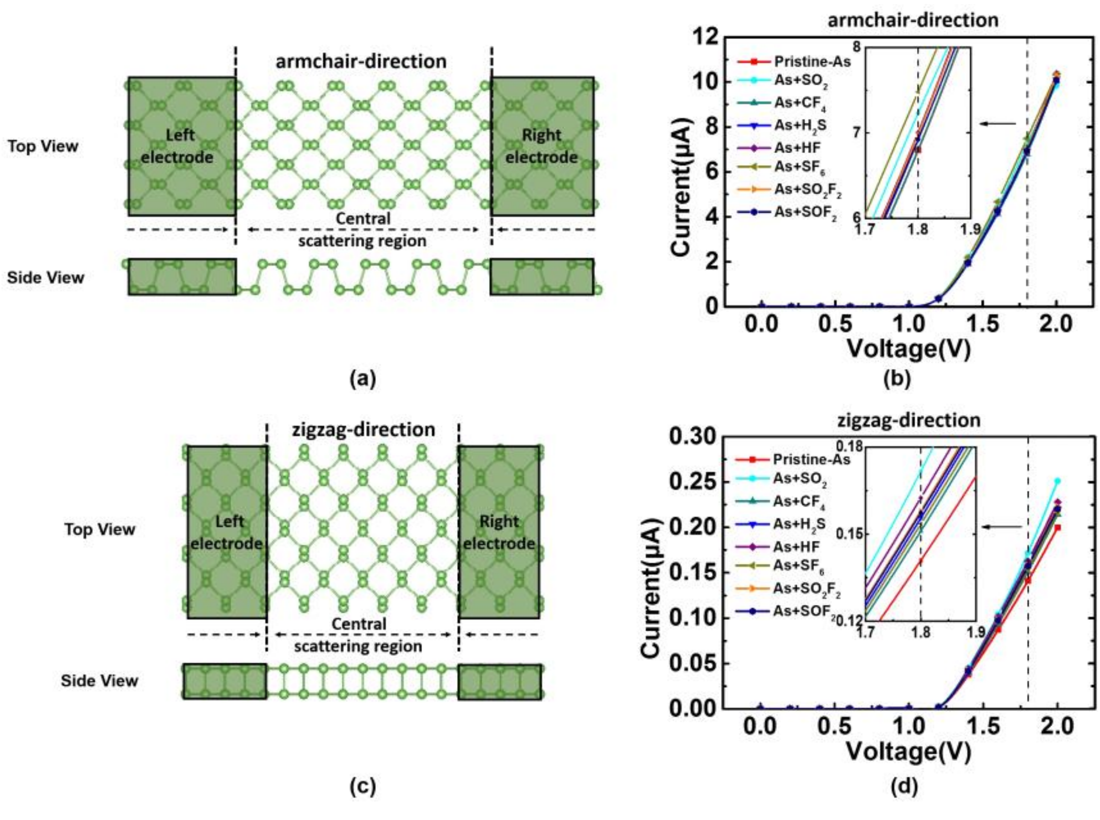

Figure 5 (color online) (a, c) Schematic models of the transport devices along the armchair or zigzag direction. *I-V* relations of B-As without and with gas adsorption along the armchair (b)

and zigzag (d) directions (here, the current is half of the total current).

Adsorption-induced alternation in resistivity can also be determined experimentally and used to evaluate the performance of sensor. To allow online monitoring and direct comparison with experimental results, we explicitly calculate the *I-V* relations before and after the adsorptions of the decompositions of SF_6. Due to the anisotropic feature of B-As shown in Figure 5, two-terminal transport models along both armchair and zigzag directions are considered. Perpendicular to the transport direction, periodic boundary conditions are imposed. Supercells of 2×3 (3×2) and 5×3 (3×5) are used for the electrode and scattering regions, respectively, for the armchair (zigzag) direction. Generally, the electron transport properties of 2D materials are determined by the band alignments and the inter- and intraband transitions around the Fermi level.[43] On the one hand, current can only be generated from the electronic states within the bias window;[44] on the other hand, the dispersion of the bands[33] and parity limitations,[45] are also critical for the electron transport properties. Our previous work[29] systematically studied the transport properties of pristine B-As and revealed its anisotropic characteristics along the armchair and zigzag directions.

In order to quantitatively evaluate the sensitivity of B-As, the sensor response (S) is introduced and defined as $S = [|R - R_0|/R_0] \times 100\%$, where R and R_0 are the resistances of B-As with and without gas adsorbate, respectively.[46, 47] The *I-V* relations before and after gas adsorption under bias from 0 to 2 V along both directions are depicted in Figure 5(b) and (d). As seen from the inset of Figure 5(b), there is a current increase from 6.95 to 7.23 μA at a bias of 1.8 V with a response S = 3.9% after the adsorption of SO_2 along the armchair direction. A comparably higher response is found for SF_6 at 1.8 V as the current increases from 6.95 to 7.48 μA. On the other hand, a significantly higher S = 18% is found for SO_2 along the zigzag direction with a current increase from 0.141 to 0.172 μA under a bias of 1.8 V. This response can be further enhanced to 20.4% under a bias voltage of 2.0 V.

In addition to defects and doping, lattice strain has been shown to be an effective approach for manipulating the electronic,[30] transport,[48, 49] optical,[50] and thermal properties[51, 52] of 2D semiconductors. Herein, we study the effects of equibiaxial tensile strain, which is applied to both the electrode and the central scattering regions. Figure S3 (a, b) shows that for a given value of bias voltage, the resulting current depends strongly on the applied strain. The *I-V* characteristics along both directions show a nonmonotonic dependence on strain, which is similar to the behavior of graphene nanoribbons under uniaxial strain.[48] A similar variation in anisotropic electrical conductance was reported for B-P.[53] Based on the above discussion on the adsorption energy, charge transfer, work function, recovery time, and *I-V* relations, B-As is found to be very promising for SO_2 detection. Therefore, we further discuss the strain effects on sensing SO_2 molecules.

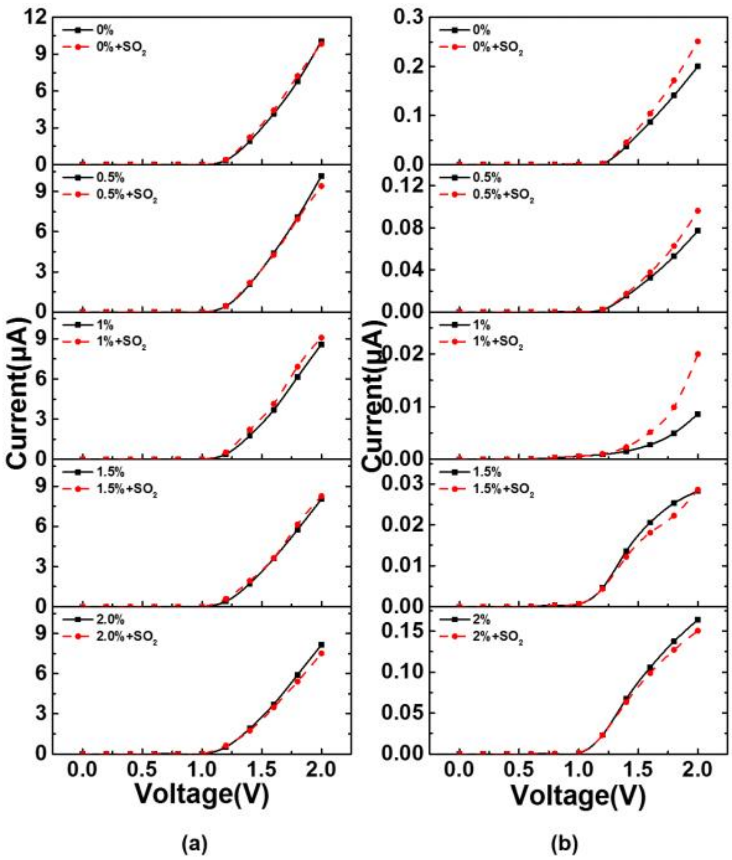

Figure 6 (color online) *I-V* relations of B-As without and with SO_2 adsorption along the (a) armchair and (b) zigzag directions under different equibiaxial tensile strains (here, the current is half of the total current)

Figure 6 shows that the strain response of the *I-V* relation along the armchair direction is relatively weak. However, the current passing through the zigzag direction can be increased from 8.62 to 20 nA at 2.0 V bias voltage, which corresponds to a response S = 132%, under a 1% equibiaxial tensile strain. The large response of B-As to an SO_2 molecule under strain may facilitate the corresponding sensing applications, whereas delicate strain control is needed as the predicted large S only exists in a narrow range of strain. The *I-V* relations under larger strains can be found in Figure S4 of the Supplemental Material.

Conclusion

In summary, we investigated the structural, electronic, and transport properties of B-As adsorbing the decompositions of SF_6 based on first-principles calculations combined with NEGF. Our results show that SO_2 has a relatively strong adsorption strength, which may be attributed to the significant charge transfer between SO_2 and B-As. Moreover, the adsorption strengths of SO_2, SOF_2, and HF can be enhanced under an *E*-field, and their adsorption can significantly increase the work function. The *I-V* characteristics show that the adsorption of SO_2 can induce a larger response than the other decompositions of SF_6, especially along the zigzag direction. The response of B-As to SO_2 can be significantly enhanced under a small equibiaxial tensile strain. These results may offer perspectives on the application of B-As as a sensor for SO_2 molecules among the decompositions of SF_6.

Supplemental Material

Potential adsorption configurations before and after structural optimization; adsorption properties of SO_2 on different 2D materials; bond lengths of the gas molecules before and after adsorption; recovery time at room temperature; TDOS and LDOS projected on the gas molecules; adsorption properties of gas molecules using different supercells; *I-V* relations of B-As under different equibiaxial tensile strains; *I-V* relations of B-As without and with SO_2 adsorption under strains.

NOTES

The authors declare no competing financial interests.

ACKNOWLEDGEMENTS

This work is supported by the Research Grants Council of Hong Kong (17300018 and 17201019), the National Natural Science Foundation of China (51706192 and 11874313), and the Zhejiang Provincial Natural Science Foundation (LR19A040001), and the Environment and Conservation Fund (69/2018). The authors are grateful for the research computing facilities offered by ITS, HKU.

References:

[1] Srivastava K D and Morcos M M 2001 A review of some critical aspects of insulation design of GIS/GIL systems. In: *Transmission and Distribution Conference and Exposition, 2001 IEEE/PES,*

[2] Xiaoxing, Z.; Yao, Y.; Ju, T.; Caixin, S.; Linyun, W., Actuamity and Perspective of Proximate Analysis of SF_6 Decomposed Products under Partial Discharge. *High Voltage Eng.* **2008**, 4, 37-42.

[3] Cai, T.; Wang, X. P.; Huang, Y. G.; Du, S. Y., Infrared Spectrum Analysis of SF_6 and SF_6 Decomposition. *Spectrosco. & Spec. Anal.* **2010**, *30*, 2967.

[4] Beyer, C.; Jenett, H.; Klockow, D., Influence of Reactive SF_x Gases on Electrode Surfaces after Electrical Discharges under SF_6 Atmosphere. *Dielec. & Elec. Insul. IEEE Trans. 2000, 7, 234-240.*

[5] Fu, Y.; Yang, A.; Wang, X.; Murphy, A. B.; Li, X.; Liu, D.; Wu, Y.; Rong, M., Theoretical Study of the Neutral Decomposition of SF_6 in the Presence of H_2O and O_2 in Discharges in Power Equipment. *J Phys. D: Appl. Phys.* **2016**, *49*, 385203

[6] Tsai, W. T., The Decomposition Products of Sulfur Hexafluoride (SF_6): Reviews of Environmental and Health Risk Analysis. *J Fluorine Chem.* **2007**, *128*, 1345-1352.

[7] Tang, J.; Yang, X.; Yao, Q.; Miao, Y.; She, X.; Zeng, F., Correlation Analysis between SF_6 Decomposed Components and Negative Dc Partial Discharge Strength Initiated by Needle-Plate Defect. *IEEJ Transac. on Elec. & Electro. Eng.* **2018***, 13, 382-389.*

[8] Luo, J.; Fang, Y. H.; Su, Z. X.; Li, D. C.; Zhao, Y. D.; Wang, A. J.; Wu, J.; Cui, F. X.; Li, Y. Y., The Research of Temperature Properties of Photoacoustic Spectroscopy Detection for SF_6 Decomposition Products in Gas Insulated Switchgear. *Anal. Methods* **2015**, *7*, 3806-3813.

[9] Jong; Edmund; C.; Luxbacher; Kray; D.; Macek; Paul; V.; McNair, Ultra-Trace Analysis Technique for SF_6 Using Gas Chromatography with Negative Ion Chemical Ionization Mass Spectrometry. *J Chromatogr. Sci.* **2015,** *6*. 854-859.

[10] Ming, D.; Zhang, C.; Ming, R.; Ricardo, A.; Ye, R., Electrochemical and Infrared Absorption Spectroscopy Detection of Sf_6 Decomposition Products. *Sensors* **2017**, *17*, 2627.

[11] Meng, Z.; Stolz, R. M.; Mendecki, L.; Mirica, K. A., Electrically-Transduced Chemical Sensors Based on Two-Dimensional Nanomaterials. *Chem. Rev.* **2019***, 119, 478-598.*

[12] Donarelli, M.; Ottaviano, L., 2D Materials for Gas Sensing Applications: A Review on Graphene Oxide, MoS_2, WS_2 and Phosphorene. *Sensors* **2018**, *18*. 3638

[13] Schedin, F.; Geim, A.; Morozov, S.; Hill, E.; Blake, P.; Katsnelson, M.; Novoselov, K., Detection of Individual Gas Molecules Adsorbed on Graphene. *Nat. Mat.* **2007***, 6, 652.*

[14] Zhang, Y.H.; Chen, Y.-B.; Zhou, K.G.; Liu, C.H.; Zeng, J.; Zhang, H.L.; Peng, Y., Improving Gas Sensing Properties of Graphene by Introducing Dopants and Defects: A First-Principles Study. *Nanotechnology* **2009**, *20*, 185504.

[15] Kong, X.K.; Chen, C.L.; Chen, Q.W., Doped Graphene for Metal-Free Catalysis. *Chem. Soc. Rev.* **2014**, *43*, 2841-2857.

[16] Zhang, S.; Xie, M.; Li, F.; Yan, Z.; Li, Y.; Kan, E.; Liu, W.; Chen, Z.; Zeng, H., Semiconducting Group 15 Monolayers: A Broad Range of Band Gaps and High Carrier Mobilities. *Angew. Chem.* **2016**, *128*, 1698-1701.

[17] Zhang, S.; Guo, S.; Chen, Z.; Wang, Y.; Gao, H.; Gómez-Herrero, J.; Ares, P.; Zamora, F.; Zhu, Z.; Zeng, H., Recent Progress in 2D Group-VA Semiconductors: From Theory to Experiment. *Chem. Soc. Rev.* **2018**, *47*, 982-1021.

[18] Kou, L.; Frauenheim, T.; Chen, C., Phosphorene as a Superior Gas Sensor: Selective Adsorption and Distinct I–V Response. *J Phys. Chem. Lett.* **2014***, 5,* 2675-2681

[19] Kistanov, A. A.; Khadiullin, S. K.; Dmitriev, S. V.; Korznikova, E. A., A First-Principles Study on the Adsorption of Small Molecules on Arsenene: Comparison of Oxidation Kinetics in Arsenene, Antimonene, Phosphorene, and InSe. *ChemPhysChem* **2019**, *20*, 575-580.

[20] Cui, S.; Pu, H.; Wells, S. A.; Wen, Z.; Mao, S.; Chang, J.; Hersam, M. C.; Chen, J., Ultrahigh Sensitivity and Layer-Dependent Sensing Performance of Phosphorene-Based Gas Sensors. *Nat. Commun.* **2015**, *6*, 8632.

[21] Wang, G.; Slough, W. J.; Pandey, R.; Karna, S. P., Degradation of Phosphorene in Air: Understanding at Atomic Level. *2D Mater.* **2016**, *3*, 025011.

[22] Ziletti, A.; Carvalho, A.; Trevisanutto, P.; Campbell, D.; Coker, D.; Neto, A. C., Phosphorene Oxides: Bandgap Engineering of Phosphorene by Oxidation. *Phys. Rev. B* **2015**, *91*, 085407.

[23] Safari, F.; Moradinasab, M.; Fathipour, M.; Kosina, H., Adsorption of the NH_3, NO, NO_2, CO_2, and CO Gas Molecules on Blue Phosphorene: A First-Principles Study. *Appl. Surf. Sci.* **2019**, *464*, 153-161.

[24] Lei, T.; Liu, C.; Zhao, J. L.; Li, J. M.; Li, Y. P.; Wang, J. O.; Wu, R.; Qian, H. J.; Wang, H. Q.; Ibrahim, K., Electronic Structure of Antimonene Grown on Sb_2Te_3 (111) and Bi_2Te_3 Substrates. *J Appl. Phys.* **2016**, *119*, 1757-1761.

[25] Tsai, H. S.; Wang, S. W.; Hsiao, C. H.; Chen, C. W.; Ouyang, H.; Chueh, Y. L.; Kuo, H. C.; Liang, J. H., Direct Synthesis and Practical Bandgap Estimation of Multilayer Arsenene Nanoribbons. *Chem. Mater.* **2016**, *28*, 425-429.

[26] Liu, C.; Liu, C.-S.; Yan, X., Arsenene as a Promising Candidate for NO and NO_2 Sensor: A First-Principles Study. *Phys. Lett. A* **2017**, *381*, 1092-1096.

[27] Kamal, C.; Ezawa, M., Arsenene: Two-Dimensional Buckled and Puckered Honeycomb Arsenic Systems. *Phys. Rev. B* **2014**, *91*, 849-855.

[28] Chen, Y.; Chen, C.; Kealhofer, R.; Liu, H.; Yuan, Z.; Jiang, L.; Suh, J.; Park, J.; Ko, C.; Choe, H. S., Black Arsenic: A Layered Semiconductor with Extreme in-Plane Anisotropy. *Adv. Mater.* **2018**, *30*, 1800754

[29] Mao, J.; Chen, Y., Black Arsenene as a Promising Anisotropic Sensor with High Sensitivity and Selectivity: Insights from a First-Principles Investigation. *J Mater. Chem. C* **2020**, *8*, 4073-4080.

[30] Mardanya, S.; Thakur, V. K.; Bhowmick, S.; Agarwal, A., Four Allotropes of Semiconducting Layered Arsenic Which Switch into a Topological Insulator Via an Electric Field: A

Computational Study. *Phys. Rev. B* **2016**, *94*, 035423.

[31] Sun, Y.; Dong, W.; Shuai, Z., Puckered Arsenene: A Promising Room-Temperature Thermoelectric Material from First-Principles Prediction. *J Phys. Chem. C* **2017**, 35, 19080-19086.

[32] Mao, J.; Chen, Y., Band Engineering and Hybridization of Competing Arsenene Allotropes: A Computational Study. *Phys. Chem. Chem. Phys.* **2019**, *44*, 24499-24505.

[33] Zhong, M.; Xia, Q.; Pan, L.; Liu, Y.; Chen, Y.; Deng, H. X.; Li, J.; Wei, Z., Thickness-Dependent Carrier Transport Characteristics of a New 2D Elemental Semiconductor: Black Arsenic. *Adv. Funct. Mater.* **2018**, *28*, 1802581.

[34] Yang X-Y, Hussain T, Wärnå J P A, Xu Z and Ahuja R Exploring Janus MoSSe monolayer as a workable media for SOF_6 decompositions sensing based on DFT calculations *Comp. Mater. Sci*. **2021**, 186, 109976

[35] Singh A, Bae H, Lee S, Shabbiri K, Hussain T and Lee H. Highly sensitive and selective sensing properties of modified green phosphorene monolayers towards SF_6 decomposition gases *Appl. Surf. Sci.* **2020,** 512, 145641

[36] Kresse, G.; Furthmüller, J., Efficient Iterative Schemes for Ab Initio Total-Energy Calculations Using a Plane-Wave Basis Set. *Phys. Rev. B* **1996**, *54*, 11169.

[37] Perdew, J. P.; Burke, K.; Ernzerhof, M., Generalized Gradient Approximation Made Simple. *Phys. Rev. Lett* **1996**, *77*, 3865.

[38] Blöchl, P. E., Projector Augmented-Wave Method. *Phys. Rev. B* **1994**, *50*, 17953.

[39] Brandbyge, M.; Mozos, J.-L.; Ordejón, P.; Taylor, J.; Stokbro, K., Density-Functional Method for Nonequilibrium Electron Transport. *Phys. Rev. B* **2002**, *65*, 165401.

[40] Guo, S.; Yuan, L.; Liu, X.; Zhou, W.; Song, X.; Zhang, S., First-Principles Study of SO_2 Sensors Based on Phosphorene and Its Isoelectronic Counterparts: GeS, GeSe, SnS, SnSe. *Chem. Phys. Lett.***2017**, *686*, 83-87.

[41] Guo, H.; Zhang, W.; Lu, N.; Zhuo, Z.; Zeng, X. C.; Wu, X.; Yang, J., CO_2 Capture on *h*-BN Sheet with High Selectivity Controlled by External Electric Field. *J. Phys. Chem. C* **2015**, *119*, 6912-6917.

[42] Yu, X.-f.; Li, Y.-c.; Cheng, J.-b.; Liu, Z.-b.; Li, Q.-z.; Li, W.-z.; Yang, X.; Xiao, B., Monolayer Ti_2CO_2: A Promising Candidate for NH_3 Sensor or Capturer with High Sensitivity and Selectivity. *ACS Appl. Mater. Inter.* **2015**, *7*, 13707-13713.

[43] Datta, S., *Electronic Transport in Mesoscopic Systems*; Cambridge university press, 1997.

[44] Ni, Z.; Zhong, H.; Jiang, X.; Quhe, R.; Luo, G.; Wang, Y.; Ye, M.; Yang, J.; Shi, J.; Lu, J., Tunable Band Gap and Doping Type in Silicene by Surface Adsorption: Towards Tunneling Transistors. *Nanoscale* **2014**, *6*, 7609-7618.

[45] Li, Z.; Qian, H.; Wu, J.; Gu, B.-L.; Duan, W., Role of Symmetry in the Transport Properties of Graphene Nanoribbons under Bias. *Phys. Rev. Lett.* **2008**, *100*, 206802.

[46] Pour G B and Aval L F Monitoring of hydrogen concentration using capacitive nanosensor in a 1% H_2–N_2 mixture *Micro & Nano Lett.* **2018**, 13, 149-53

[47] Aval L F Influence of oxide film surface morphology and thickness on the properties of gas sensitive nanostructure sensor *Indian Journal of Pure & Applied Physics (IJPAP)* **2019**, 57, 743-9

[48] Topsakal, M.; Bagci, V.; Ciraci, S., Current-Voltage ($I-V$) Characteristics of Armchair Graphene Nanoribbons under Uniaxial Strain. *Phys. Rev. B* **2010**, *81*, 205437

[49] Xiong, F.; Tan, H. B.; Xia, C.; Chen, Y., Strain and Doping in Two-Dimensional Snte Nanosheets: Implications for Thermoelectric Conversion. *ACS Appl. Nano Mater.* **2019**, *3*, 114-119..

[50] Yang, L.; Cui, X.; Zhang, J.; Wang, K.; Shen, M.; Zeng, S.; Dayeh, S. A.; Feng, L.; Xiang, B., Lattice Strain Effects on the Optical Properties of MoS_2 Nanosheets. *Sci. Rep.* **2014**, *4*, 5649.

[51] Li, S.; Ma, J.; Pei, Y.; Chen, Y., Anharmonic Lattice Dynamics of Te and Its Counter-Intuitive Strain Dependent Lattice Thermal Conductivity. *J Mater. Chem. C* **2019**, *7*, 5970-5974.

[52] Zeng, Z.; Tadano, T.; Chen, Y., Anharmonic Lattice Dynamics and Thermal Transport of Monolayer Inse under Equibiaxial Tensile Strains. *J Phys. Condens. Matter* **2020**.

[53] Fei, R.; Yang, L., Strain-Engineering the Anisotropic Electrical Conductance of Few-Layer Black Phosphorus. *Nano Lett.* **2014**, *14*, 2884-2889.